Composition–Property Correlations in PM6:Y6:ITIC-M Cascade Solar Cells: Energy Levels, Trap Density, and Dielectric Permittivity

Habib Kazemi Chubi[a, b], Davoud Raeyani[c, d], Asghar Asgari[c, e,*]

[a]Faculty of Physics, University of Tabriz, Tabriz, Iran,
[b]Department of Physics, Osku Islamic Azad University, Osku, Iran,
[c]Photonics Devices Research Group, Research Institute of Applied Physics and Astronomy, University of Tabriz, Tabriz, Iran,
[d]Instituto de Ciencia de Materiales (ICMUV) Universidad de Valencia, Catedrático José Beltrán, Spain,
[e]School of Electrical, Electronic, and Computer Engineering, University of Western Australia, Crawley, Australia.

Corresponding author email: asgari@tabrizu.ac.ir

Received: Feb. 02, 2026, Revised: Mar. 13, 2026, Accepted: Mar. 15, 2026, Available Online: Mar. 17, 2026.
DOI: Due to the current conditions, there is no possibility to buy DOI for papers. We hope to buy them as soon as possible.

ABSTRACT— Despite decades of research on ternary organic solar cells, accurate prediction and precise definition of their blend properties remain challenging. In this work, we investigate the interdependence between composition ratio and optoelectronic properties in a PM6:Y6:ITIC-M cascade-type ternary organic solar cell using drift–diffusion simulations combined with experimental parameters. Key parameters, including effective bandgap, electron affinity, dielectric permittivity, doping density, and trap density, were extracted and modeled as functions of the ITIC-M weight percentage. Comprehensive characterization through morphological analysis (RMS roughness), electrical measurements (carrier mobility), and photovoltaic performance metrics revealed strong correlations with the dielectric permittivity (ε), enabling more accurate predictions. The proposed predictive model establishes a direct link between blend ratio and performance parameters—such as mobility and surface roughness—thus providing valuable guidance for optimizing ternary organic photovoltaic materials in future research.

KEYWORDS: cascade, drift-diffusion, optoelectronic parameters, Ternary.

I. INTRODUCTION

Organic solar cells (OSCs) based on small-molecule donors and acceptors have rapidly evolved in recent years, offering promising solutions for lightweight, flexible, and solution-processable photovoltaic applications [1]–[3]. Recent advancements have pushed their power conversion efficiencies (PCEs) toward the commercial benchmark of 20% [4]. Bulk heterojunction (BHJ) architectures optimize exciton dissociation and charge transport by mixing electron donor and acceptor materials. However, these systems face trade-offs between optical absorption and energy level alignment, which constrain their performance [5],[6].

Various strategies to boost device efficiency can be classified into two main parts: active layer and material modifications [7],[8], and transport layer and electrode modifications [9],[10]. Ternary blend engineering is a method where a third component is added to the donor–acceptor matrix, which has shown compelling improvements in light harvesting, charge dynamics, and morphological control [11]–[13]. Ternary organic solar cells (TOSCs) enable simultaneous improvements in the

short-circuit current density (J_{SC}), open-circuit voltage (V_{OC}), fill factor (FF), power conversion efficiency (PCE), and stability by modulating the molecular packing and interfacial interactions [14],[15]. Recent research emphasizes that TOSCs are not simple extensions of binary cells. Small-molecule donors, such as DR3TBDTT derivatives, have demonstrated that compositional variations can transform nanoscale morphology and energy-level alignment [16]. Additionally, a ternary composition of PM6:Y6:ITIC-M has broadened our understanding of how the incorporation of ITIC-M enhances the electronic properties, suppresses charge recombination loss, and optimizes the surface morphology [17]. Therefore, TOSCs are ideal solutions for addressing problems related to interfacial charge transfer states, trap-assisted recombination, and morphology-induced disorder [18],[19].

Ternary systems introduce novel phenomena, such as cascade energy transfer, energy-level tuning, and alloy-like mixing behaviors [20]. Each model explains how the three components interact electronically and structurally. These effects can enhance exciton dissociation, suppress charge recombination, and improve the FF, leading to higher PCE. In particular, cascade-like systems benefit from intermediate energy levels that facilitate exciton dissociation and broaden the absorption window [21]. In contrast, alloy-like blends enable tunable V_{OC} and charge-transfer (CT) state energies through electronic mixing [22],[23]. While past studies have reported shifts in energy levels and morphology, few have provided analytical relationships between blend composition and key device-relevant quantities, such as energy levels, trap densities, or dielectric constants.

In this study, we investigated the PM6:Y6:ITIC-M ternary blend to establish correlations between the compositional ratio and optoelectronic properties, including the energy levels, dielectric permittivity (ε), trap densities (Nt1 and Nt2), and doping density (Ndoping). We developed a formula for predicting the effect of the ITIC-M concentration on the bandgap and electron affinity. Additionally, the variation of the dielectric permittivity with varying weight ratios of ITIC-M was compared with the roughness, carrier mobility, carrier lifetime, and FF of the solar cell device to establish a predictive relation for the permittivity of the ternary blend. The recombination dynamics of solar cell devices at different ITIC-M concentrations were also simulated. The results highlight how morphology and defects jointly can shape the device performance and provide insights into future ternary solar cell designs. Our findings establish predictive correlations between the ternary blend composition and device performance, highlighting the optimal ranges for charge transport and defect minimization.

II. MATERIALS AND METHODS

The simulation focused on fitting the experimental current-voltage curves and studying the resulting changes in the properties of the active layer by varying the ternary blend weight ratio. We selected fitting parameters including bandgap, electron affinity, dielectric permittivity, trap densities, and doping density, while considering all other parameters constant for each solar cell (Fig. 1(a)). The donor-to-acceptor weight ratio of the ternary layer was fixed at 1:1.2 (Fig. 1(b)), and systematic variations were made in the concentrations of the two acceptor materials. The SCAPS-1D software [24], based on the principles of drift-diffusion (DD) theory, was used to simulate the solar cell device performance. The DD theory involves solving the Poisson and continuity Eq. (1) to Eq. (3) [25]:

$$\frac{d^2\psi(x)}{dx^2} = -\frac{q}{\varepsilon_0 \varepsilon} \times \left[-n(x) + p(x) - N_A^- + N_D^+ + \rho_p - \rho_n\right] \quad (1)$$

where ψ is the electrostatic potential, q is the electrical charge, ε and ε_0 are, respectively, the dielectric permittivity and the vacuum permittivity, and n and p are electron and hole concentrations, respectively. The N_A^- and N_D^+ represent the dopant concentrations, respectively. ρ_n and ρ_p are the electron and hole distributions, respectively. The continuity

equations for electrons and holes are Eq. (2) and Eq. (3):

$$\frac{dJ_n}{dx} = G_n - R_n \tag{2}$$

$$\frac{dJ_p}{dx} = G_p - R_p \tag{3}$$

where J_n and J_p are electron and hole current densities, respectively. The recombination and generation rates are given by R and G. The carrier transport can be expressed by Eqs. (4) and (5) [26]:

$$J_n = qD_n \frac{dn}{dx} - q\mu_n n \frac{d\psi(x)}{dx} \tag{4}$$

$$J_p = -qD_p \frac{dp}{dx} - q\mu_p p \frac{d\psi(x)}{dx} \tag{5}$$

where D_n and D_p are electron and hole diffusion coefficients. Also, μ_n and μ_p are the electron and hole mobilities. Solving these basic semiconductor equations under steady-state conditions has enabled the achievement of performance parameters for solar cells. The SCAPS package solves the Poisson and continuity equations by a finite difference method using the Gummel iteration scheme [27].

Device parameters are summarized in Table 1, obtained from references [28]–[30], while data related to fitting parameters are summarized in Table 2. The cascade band structure of the ternary blend used in this simulation is illustrated in Fig. 2(a). Using previously reported experimental parameters, we analyzed the effective bandgap variations of the active layer relative to the transport layers (Fig. 2(b)). We utilized absorption spectra of active layers with different weight ratios of ITIC-M [17] and the AM1.5G 1 sun spectrum for light intensity, as depicted in Fig. 3. We introduced two types of defect states into all solar cells: interfacial defects and active layer defects. The distribution of defects in the active layer was modeled using the Gaussian distribution equation [31].

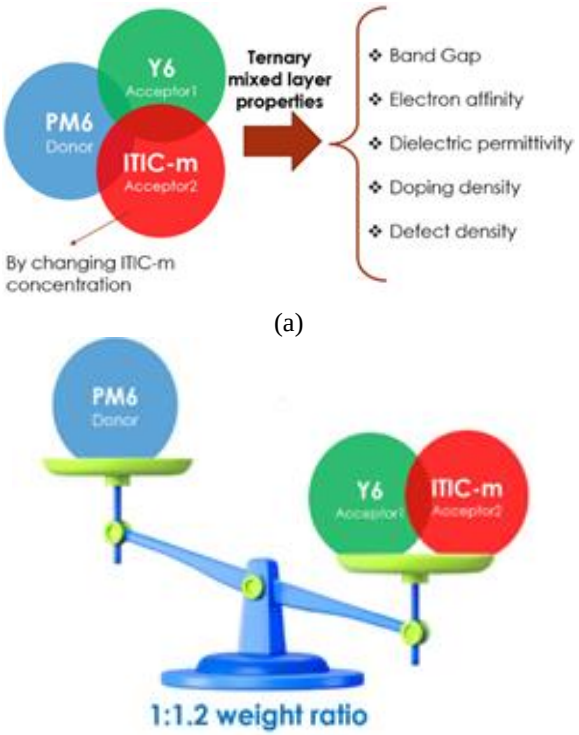

Fig. 1. (a) Schematic of ternary blend and properties were focused on, (b) Weight ratio of the donor and acceptor components in the ternary compound.

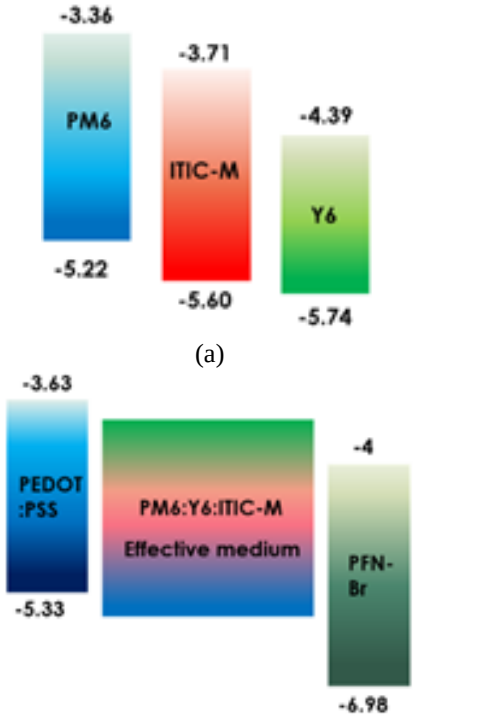

Fig. 2. Band structure of (a) active layer ternary cascade structure and (b) solar cell device structure.

Table 1. Material parameters used for solar cell device simulation.

Parameters	Materials		
	PEDOT: PSS [28]	Ternary [17],[30]	PFN-Br [29]
Thickness (nm)	50	Experimental	10
Bandgap (eV)	1.7	Fitting and Experimental	2.98
Electron affinity (eV)	3.63	Fitting	4
Dielectric permittivity	3	Fitting	5
Conduction Band Density of States (N_c) (cm^{-3})	1×10^{19}	1×10^{21}	1×10^{19}
Valence Band Density of States (N_v) (cm^{-3})	1×10^{19}	1×10^{19}	1×10^{19}
Electron mobility (cm^2/Vs)	9×10^{-3}	Experimental	1×10^{-4}
Hole mobility (cm^2/Vs)	9×10^{-3}	Experimental	2×10^{-6}
Donor density (cm^{-3})	0	Fitting	9×10^{18}
Acceptor density (cm^{-3})	3×10^{17}	0	0
Defect Density (cm^{-3})	1×10^{11}	Fitting	1×10^{14}

Table 2. Fitting parameters of the active layer used for simulation.

Parameters	PM6:Y6(100-x): ITIC-M(x)					
	0%	5%	10%	20%	50%	100%
Bandgap (eV)	1.4	1.406	1.414	1.434	1.44	1.665
Electron affinity (eV)	4.1	4.086	4.07	4.058	4.025	3.908
Dielectric permittivity	3.8	6.58	6.48	3.94	3.03	2.5
Electron mobility ($\times10^{-4}cm^2$/Vs)	5.08	7.13	5.89	3.94	2.00	3.62
Hole mobility ($\times10^{-4}cm^2$/Vs)	6.83	8.19	6.91	4.04	2.62	1.96
Donor density (cm^{-3})	5.3×10^{17}	4.5×10^{17}	3.26×10^{17}	2.7×10^{17}	9.36×10^{16}	8.77×10^{15}
Defect Density (cm^{-3}) Nt1	2.66×10^{13}	3.46×10^{12}	4.3×10^{13}	4.28×10^{13}	7.65×10^{13}	7.67×10^{14}
Defect Density (cm^{-3}) Nt2	1×10^{13}	2.76×10^{9}	1×10^{9}	1.3×10^{10}	3.8×10^{10}	3.86×10^{12}

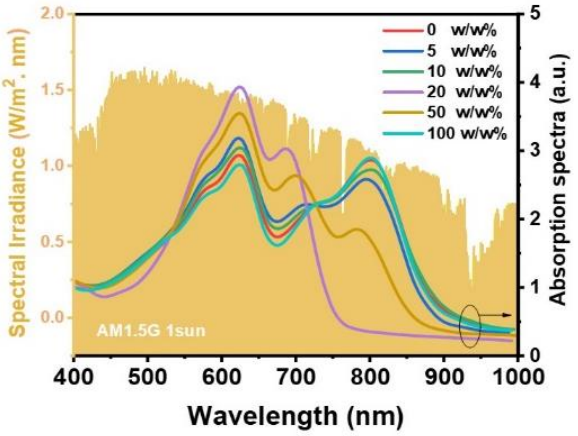

Fig. 3. Solar radiation spectrum and the absorption spectra of the ternary blend with different weight ratios of ITIC-M.

III. Results and Discussion

The current densities for different weight ratios of ITIC-M along with the simulated fitting curves for each composition are shown in Fig. 4. Based on this figure, the fitted curves are in excellent agreement with the experimental curves. The chi-square values for each fitting curve ranged from 1×10^{-4} to 6×10^{-4}, demonstrating that the simulation results are very accurate and close to the experimental data.

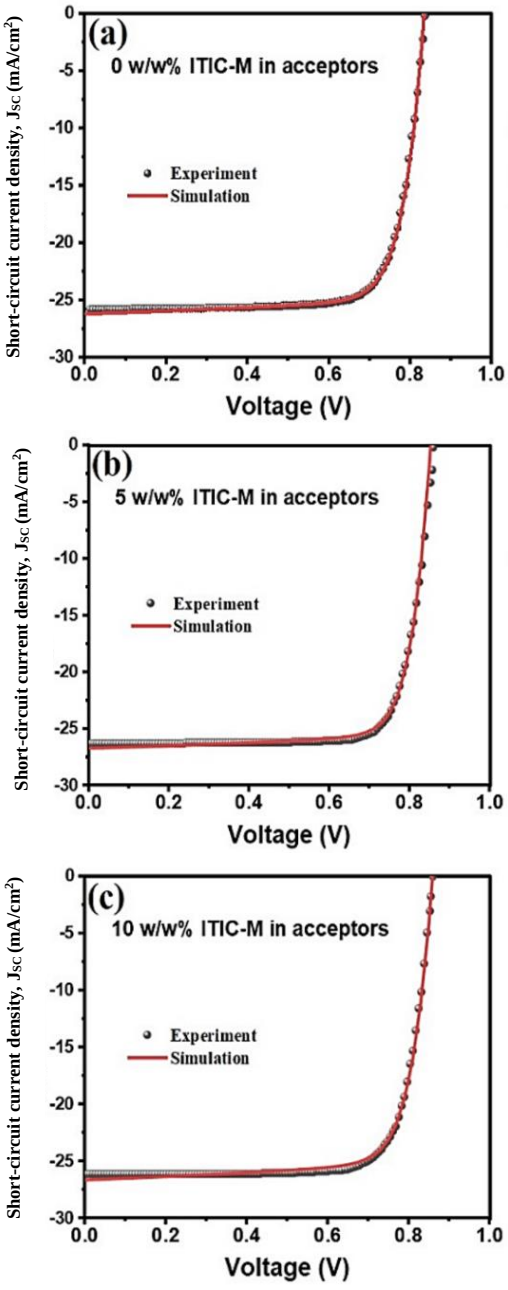

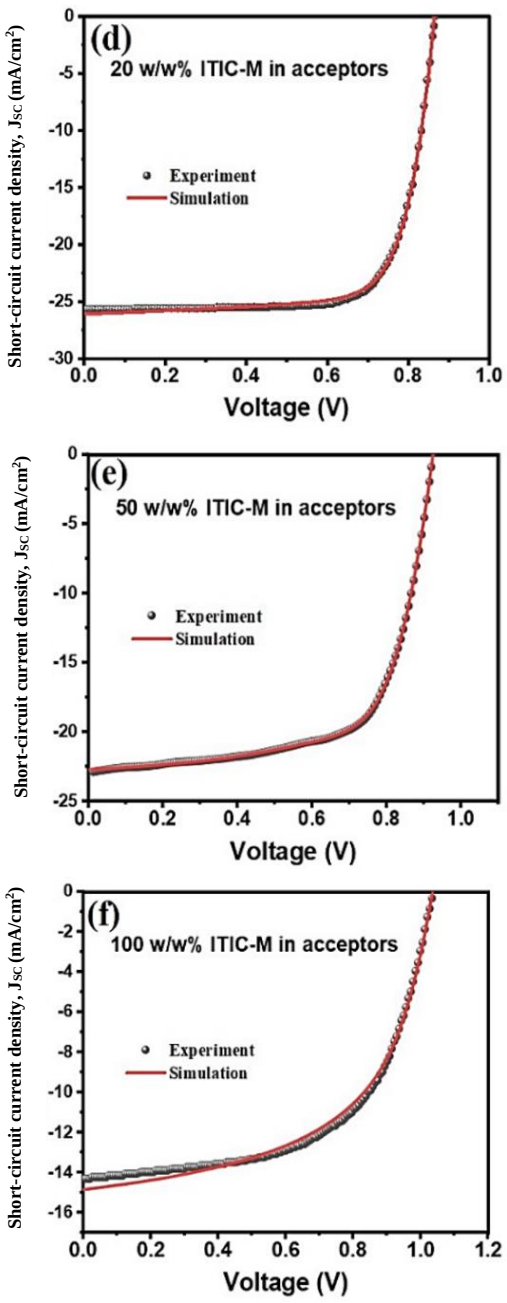

Fig. 4. Short circuit current density-voltage curves of experimental and fitting results for (a) 0 w/w%, (b) 5 w/w%, (c) 10 w/w%, (d) 20 w/w%, (c) 50 w/w%, and (f) 100 w/w% of ITIC-m in acceptors.

Additionally, the performance parameters versus weight ratios of ITIC-M are illustrated in Fig. 5, which demonstrates that the experimental and simulation results are consistent and follow a systematic trend. Analysis of different weight ratios of ITIC-M shows that, except for an anomaly at 5 wt% ITIC-M, the performance parameters follow a consistent trend. Subsequently, we developed a formalism to predict and explain this trend.

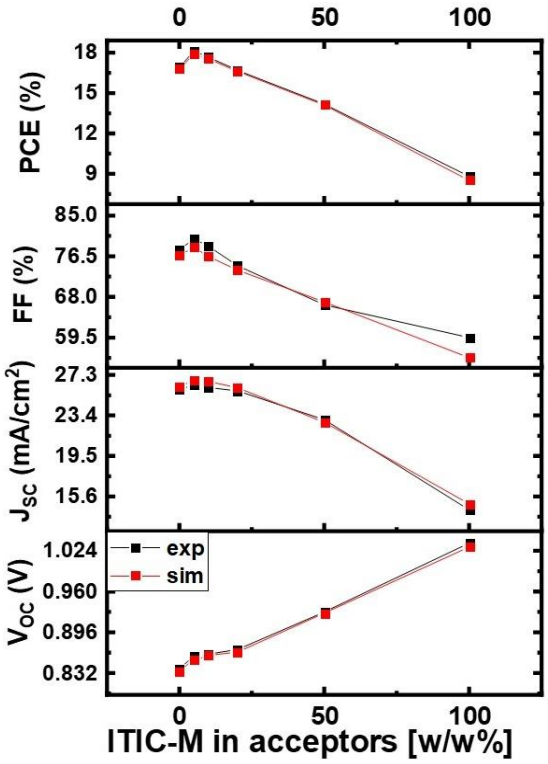

Fig. 5. Experimental and simulated solar cell performance parameters: power conversion efficiency (PCE), fill factor (FF), short-circuit current density (J_{SC}), and open-circuit voltage (V_{OC}), vs. stability of weight ratios of ITIC-M in acceptors.

In Fig. 6, the simulated parameters are shown versus weight ratios of ITIC-M in the ternary blend with curve-fitting analysis. The dielectric permittivity (ε) increased at 5 wt% and 10 wt% ITIC-M concentrations, before showing a parabolic decrease. Since ε showed a nonlinear trend, we attempted to describe and predict its behavior by relating it to experimental parameters as discussed below. The electron affinity and bandgap of the solar cells fabricated with different concentrations of ITIC-M showed cubic polynomial trends, as shown in Fig. 6(b) and Fig. 6(c). The corresponding fitting formula for electron affinity is as follows:

$$\varepsilon = A + Bx + Cx^2 + Dx^3 \quad (6)$$

where A, B, C, and D are approximately 4.1, -0.003, 4.8×10^{-5}, and -3.75×10^{-7}, respectively, and x is the ITIC-M concentration.

For the bandgap, the fitting formula is as follows:

$$E_g = A + Bx + Cx^2 + Dx^3 \quad (7)$$

where *A*, *B*, *C*, and *D* are approximately 1.4, 0.003, -6×10^{-7}, and 7×10^{-7}, respectively, and *x* is the ITIC-M concentration.

A comparison between the bandgap and electron affinity of the ternary solar cells versus ITIC-M weight ratios is shown in Fig. 7. The figure indicates that increasing the ITIC-M concentration leads to bandgap widening. Importantly, this bandgap increase occurs through approximately symmetric shifts of both the HOMO and LUMO energy levels, resulting in simultaneous changes that increase the overall bandgap of the ternary active layer.

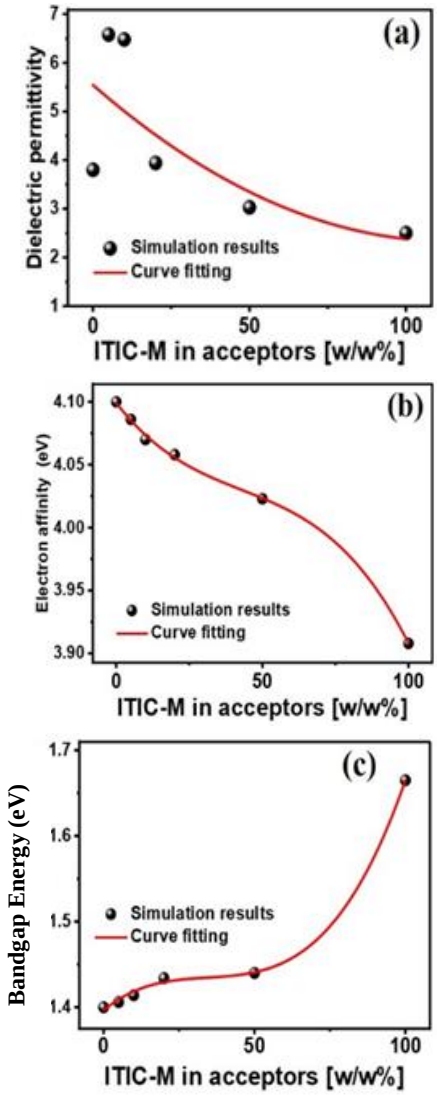

Fig. 6. Simulated parameters of (a) dielectric permittivity, (b) electron affinity, and (c) bandgap vs. weight ratios of ITIC-M in acceptors with curve-fitting.

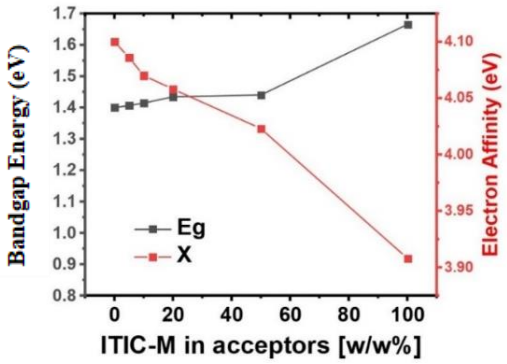

Fig. 7. Comparing simulated bandgap and electron affinity bandgap vs. weight ratios of ITIC-M in acceptors.

A comparison between the bandgap and V_{OC} of the solar cell devices is shown in Fig. 8. The figure demonstrates that the voltage loss (Eg-V_{OC}) remains approximately constant for different weight ratios of ITIC-M, indicating that energy losses do not vary significantly with ternary blend composition. Notably, at 100 wt% ITIC-M, the voltage loss reaches its maximum value, which explains the lowest PCE observed under this condition.

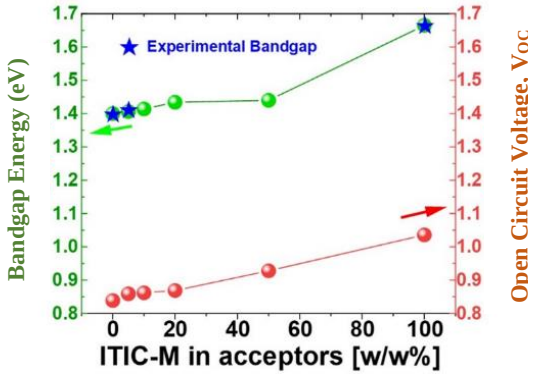

Fig. 8. Simulated and experimental bandgap of the ternary structure compared with the V_{OC} of the solar cell device, experimental data from [17],[30].

In Fig. 9, the simulated ε is compared with the FF values versus ITIC-M weight ratios. The similar trends between ε and FF suggest a correlation that may arise from the dependency of both parameters on the morphological properties of the ternary blend. Therefore, we can predict the approximate trend of FF or ε from the other's behavior, which provides better understanding of active layer morphology.

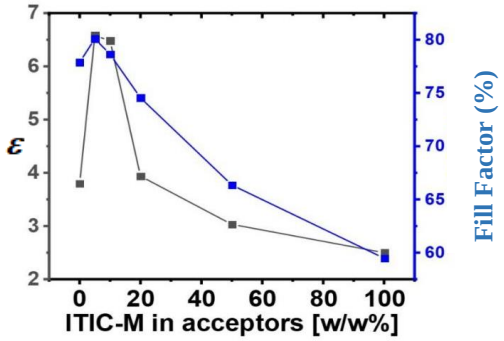

Fig. 9. Comparing simulated ε with experimental fill factor (FF) vs. weight ratios of ITIC-M in acceptors.

To explore this relationship further, the RMS roughness measured by AFM analysis for different weight ratios of ITIC-M was compared with ε (Fig. 10(a)). While there is limited correlation between the inverse of roughness and ε, some correspondence is still recognizable in the trend lines. In a separate comparison, we correlated the experimentally obtained carrier lifetime with ε (Fig. 10(b)). Although the experimental data were limited to three points, the trends showed good similarity, suggesting that morphological effects may not always manifest as obvious surface features like roughness, but rather as internal phase separation enhancements not visible at the surface.

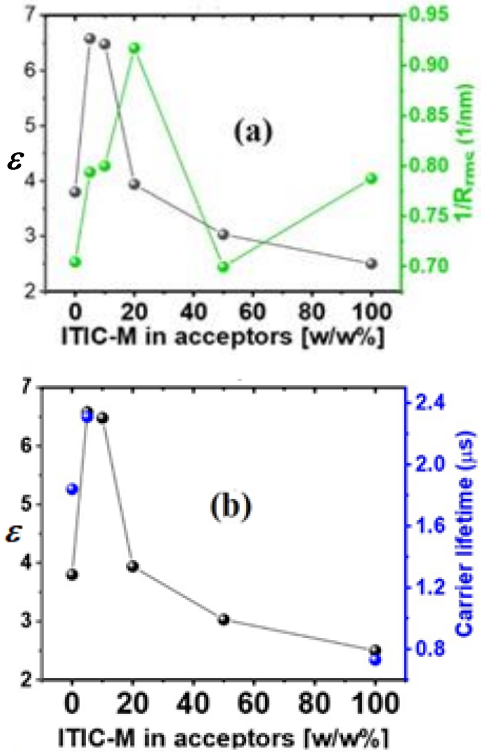

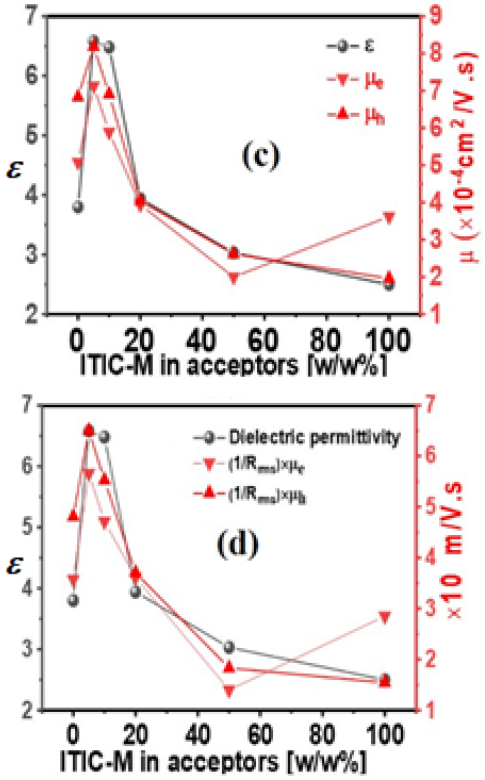

Fig. 10. Comparing simulated ε with different experimental parameters, including (a) root mean square roughness, (b) carrier lifetime, (c) carrier mobilities, and (d) coupling coefficient of ε and root mean square roughness vs. weight ratios of ITIC-M in acceptors.

Another parameter examined is the experimentally determined mobility of electrons and holes (Fig. 10(c)), which are also related to carrier lifetime. These parameters also showed good agreement with the ε trend line. Notably, hole mobility correlated better with the ε trend, indicating that this device performance is more dependent on hole transport than electron transport. Finally, by considering the product of the inverse of RMS roughness and mobility (Fig. 10(d)), we obtain improved correlation with the ε trend, demonstrating that morphological optimization involves both surface and internal phase separation enhancements.

Figure 11(a) shows that the trap densities of Nt1 (near LUMO) and Nt2 (near HOMO) increased exponentially with the ITIC-M concentration. The figure also demonstrates that the trap density of Nt1 is more significant than that of Nt2. The trap density trends upon changing the

weight ratio of ITIC-M are approximately similar for Nt1 and Nt2. The schematic representation of the trap levels within the bandgap is shown in Fig. 11(b).

Using these trap parameters, we calculated the total recombination rate for solar cell devices with different weight ratios of ITIC-M (Fig. 12). Although the total recombination rates for all devices are of the same order of magnitude, the 5 wt% sample showed the minimum recombination rate. This result confirms that 5 wt% ITIC-M is the optimal composition, as it exhibits higher efficiency compared to other weight ratios.

Additionally, Fig. 13 shows that increasing the ITIC-M concentration decreases the effective doping concentration of the active layer, suggesting that ITIC-M has lower electron-accepting ability and weaker n-type characteristics than Y6. This analysis helps in predicting and understanding how organic materials influence the overall semiconductor characteristics of the active layer and enables comparison of different material systems.

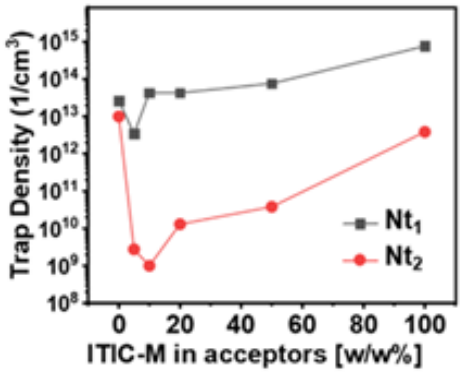

(a)

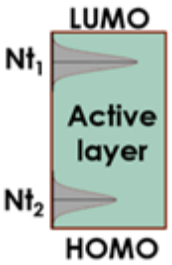

(b)

Fig. 11. (a) Trap densities for two shallow trap states within the bandgap of the ternary layer vs. weight ratios of ITIC-M in acceptors, and (b) schematic structure of the related traps.

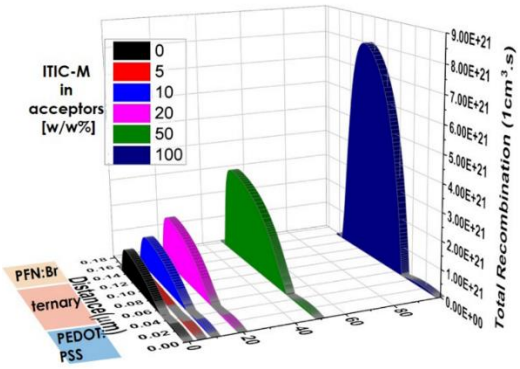

Fig. 12. Total recombination rate within the device distance.

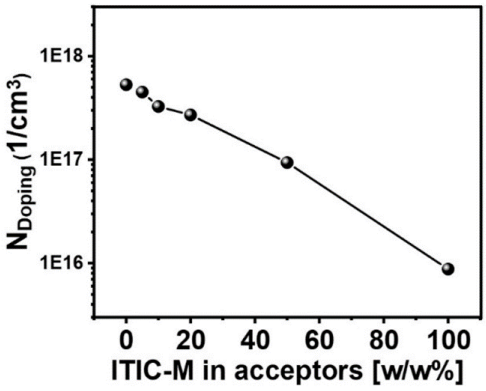

Fig. 13. Doping density of the ternary layer vs. weight ratios of ITIC-M in acceptors.

IV. Conclusion

This study focused on determining and formulating the optoelectronic properties of ternary solar cells by changing the weight ratio of the acceptor materials, thereby introducing a predictive framework for blend optimization. The results revealed that the dielectric permittivity, band structure, doping, and defect density are key parameters, enabling device simulation and fitting using only these parameters. The electron affinity and bandgap both followed cubic polynomial trends with changes in the weight ratio of ITIC-M. Both ε and FF showed similar trends, indicating that these parameters are highly related to the active layer morphology. Moreover, the strong correlation between ε and morphological properties demonstrates that ε can be accurately modeled using parameters such as RMS roughness and carrier mobility. This study contributes to ternary blend engineering by offering predictive relationships for the rapid optimization of high-efficiency OSC devices. Future studies may extend this framework to

other ternary systems or integrate additional parameters such as mobility and energy loss profiles.

REFERENCES

[1] J. Yi, G. Zhang, H. Yu, and H. Yan, "Advantages, challenges, and molecular design of different material types used in organic solar cells," Nat. Rev. Mater., Vol. 9, pp. 46-62, 2023. https://doi.org/10.1038/s41578-023-00618-1.

[2] J. Hou, O. Inganäs, R.H. Friend, and F. Gao, "Organic solar cells based on non-fullerene acceptors," Nat. Mater., Vol 17, pp. 119-128, 2018. https://doi.org/10.1038/nmat5063.

[3] K. Fukuda, K. Yu, and T. Someya, "The Future of Flexible Organic Solar Cells," Adv. Energy Mater., Vol. 10, pp. 200076510(1-10), 2020. https://doi.org/10.1002/aenm.202000765.

[4] C. Chen, L. Wang, W. Xia, K. Qiu, C. Guo, Z. Gan, J. Zhou, Y. Sun, D. Liu, W. Li, and T. Wang, "Molecular interaction induced dual fibrils towards organic solar cells with certified efficiency over 20%," Nat. Commun., Vol. 15, pp. 6865(1-10), 2024. https://doi.org/10.1038/s41467-024-51359-w.

[5] N.K. Elumalai and A. Uddin, "Open circuit voltage of organic solar cells: an in-depth review," Energy Environ. Sci. Vol. 9, pp. 391-410, 2016. https://doi.org/10.1039/C5EE02871J.

[6] R. Xue, J. Zhang, Y. Li, and Y. Li, "Organic Solar Cell Materials toward Commercialization," Small, Vol. 14, pp. 1801793(1-24), 2018. https://doi.org/10.1002/smll.201801793.

[7] L. Zhu, M. Zhang, J. Xu, C. Li, J. Yan, G. Zhou, W. Zhong, T. Hao, J. Song, X. Xue, Z. Zhou, R. Zeng, H. Zhu, C.C. Chen, R.C.I. MacKenzie, Y. Zou, J. Nelson, Y. Zhang, Y. Sun, and F. Liu, "Single-junction organic solar cells with over 19% efficiency enabled by a refined double-fibril network morphology," Nat. Mater., Vol. 21, pp. 656–663, 2022. https://doi.org/10.1038/s41563-022-01244-y.

[8] Y. Lei, Z. Liu, and L. Sun, "Ternary polymer solar cells using two nonfullerene acceptors with cascading energy level and complementary absorptions," Polymer (Guildf). Vol. 308, pp. 127376(1-7), 2024. https://doi.org/10.1016/j.polymer.2024.127376

[9] B. Olyaeefar, A. Asgari, and S. Ahmadi-Kandjani, "Effective thickness method for modeling absorption enhancement of forward-scattering nanoparticles in photovoltaic devices," Sol. Energy Mater. Sol. Cells, Vol. 215, pp. (110688(1-6), 2020. https://doi.org/10.1016/j.solmat.2020.110688.

E.A. Milani, M. Piralaee, S. Ahmadi, and A. Asgari, "The role of structural parameters on efficiency and transparency of semi-transparent non-fullerene organic solar cell," Sci. Rep. Vol. 12, pp. 14928(1-11), 2022. https://doi.org/10.1038/s41598-022-19346-7.

[10] L. Lu, T. Xu, W. Chen, E.S. Landry, and L. Yu, "Ternary blend polymer solar cells with enhanced power conversion efficiency," Nat. Photon., Vol. 8, pp. 716-722, 2014. https://doi.org/10.1038/nphoton.2014.172.

[11] L. Lu, M.A. Kelly, W. You, and L. Yu, "Status and prospects for ternary organic photovoltaics," Nat. Photonics, Vol. 9, pp. 491-500, 2015. https://doi.org/10.1038/nphoton.2015.128.

[12] D. Baran, R.S. Ashraf, D.A. Hanifi, , M. Abdelsamie, N. Gasparini, J.A. Röhr, S. Holliday, A. Wadsworth, S. Lockett, M. Neophytou, and C.J. Emmott, "Reducing the efficiency–stability–cost gap of organic photovoltaics with highly efficient and stable small molecule acceptor ternary solar cells," Nature Mater., Vol. 16, pp. 363-369, 2017.

https://doi.org/10.1038/nmat4797

[13] T. Ameri, P. Khoram, J. Min, and C.J. Brabec, "Organic Ternary Solar Cells: A Review," Adv. Mater., Vol. 25, pp. 4245-4266, 2013. https://doi.org/10.1002/adma.201300623.

[14] N. Gasparini, A. Salleo, I. McCulloch, and D. Baran, "The role of the third component in ternary organic solar cells," Nat. Rev. Mater. Vol. 4, pp. 229–242, 2019. https://doi.org/10.1038/s41578-019-0093-4.

[15] J. Zhou, Y. Zuo, X. Wan, G. Long, Q. Zhang, W. Ni, Y. Liu, Z. Li, G. He, C. Li, B. Kan, M. Li, and Y. Chen, "Solution-processed and high-performance organic solar cells using small molecules with a benzodithiophene unit," J. Am. Chem. Soc. Vol. 135, pp. 8484–8487, 2013. https://doi.org/10.1021/ja403318y.

[16] Y. Zeng, D. Li, H. Wu, Z. Chen, S. Leng, T. Hao, S. Xiong, Q. Xue, Z. Ma, H. Zhu, and Q.

Bao, "Enhanced Charge Transport and Broad Absorption Enabling Record 18.13% Efficiency of PM6:Y6 Based Ternary Organic Photovoltaics with a High Fill Factor Over 80%," Adv. Funct. Mater., Vol. 32, pp. 1-9, 2022. https://doi.org/10.1002/adfm.202110743.

[17] T.F. Hinrichsen, C.C.S. Chan, C. Ma, D. Paleček, A. Gillett, S. Chen, X. Zou, G. Zhang, H.-L. Yip, K.S. Wong, R.H. Friend, H. Yan, A. Rao, and P.C.Y. Chow, "Long-lived and disorder-free charge transfer states enable endothermic charge separation in efficient non-fullerene organic solar cells," Nat. Commun., Vol. 11, Code: 5617, pp. 1-10, 2020. https://doi.org/10.1038/s41467-020-19332-5.

[18] T. Fritsch, J. Kurpiers, S. Roland, N. Tokmoldin, S. Shoaee, T. Ferron, B.A. Collins, S. Janietz, K. Vandewal, and D. Neher, "On the Interplay between CT and Singlet Exciton Emission in Organic Solar Cells with Small Driving Force and Its Impact on Voltage Loss," Adv. Energy Mater., Vol. 12, pp. 2200641(1-11), 2022. https://doi.org/10.1002/aenm.202200641.

[19] Z. Wang, X. Zhu, J. Zhang, K. Lu, J. Fang, Y. Zhang, Z. Wang, L. Zhu, W. Ma, Z. Shuai, and Z. Wei, "From Alloy-Like to Cascade Blended Structure: Designing High-Performance All-Small-Molecule Ternary Solar Cells," J. Am. Chem. Soc., Vol. 140, pp. 1549–1556, 2018. https://doi.org/10.1021/jacs.7b13054.

J. Liu, S. Zhao, Y. Huang, Z. Xu, B. Qiao, L. Yang, Y. Zhu, Z. Li, B. Yuan, and X. Xu, "Improving charge transport and suppressing charge recombination in small molecule ternary solar cells via incorporating Bis-PC 71 BM as a cascade material," Org. Electron., Vol. 46, pp. 126-132, 2017. https://doi.org/10.1016/j.orgel.2017.03.030.

[20] R.A. Street, D. Davies, P.P. Khlyabich, B. Burkhart, and B.C. Thompson, "Origin of the Tunable Open-Circuit Voltage in Ternary Blend Bulk Heterojunction Organic Solar Cells," J. Am. Chem. Soc., Vol. 135, pp. 986-989, 2013. https://doi.org/10.1021/ja3112143.

[21] P.P. Khlyabich, B. Burkhart, and B.C. Thompson, "Compositional Dependence of the Open-Circuit Voltage in Ternary Blend Bulk Heterojunction Solar Cells Based on Two Donor Polymers," J. Am. Chem. Soc., Vol. 134, pp. 9074-9077, 2012. https://doi.org/10.1021/ja302935n.

[22] M. Burgelman, P. Nollet, and S. Degrave, "Modelling polycrystalline semiconductor solar cells," Thin Solid Films, Vol. 361, pp. 527-532, 2000. https://doi.org/10.1016/S0040-6090(99)00825-1.

[23] M. Minbashi, A. Ghobadi, M.H. Ehsani, H. Rezagholipour Dizaji, and N. Memarian, "Simulation of high efficiency SnS-based solar cells with SCAPS," Sol. Energy, Vol. 176, pp. 520-525, 2018. https://doi.org/10.1016/j.solener.2018.10.058.

[24] P.P. Altermatt, "Models for numerical device simulations of crystalline silicon solar cells - A review," J. Comput. Electron., Vol. 10, pp. 314–330, 2011. https://doi.org/10.1007/s10825-011-0367-6.

[25] S. Selberherr, *Analysis and Simulation of Semiconductor Devices*, Springer Vienna, Vienna, 1984. https://doi.org/10.1007/978-3-7091-8752-4.

[26] R. Salamatbakhsh, D. Raeyani, and A. Asgari, "Enhancing Charge Generation in Nonfullerene Interdigitated Heterojunction Organic Solar Cells," Phys. Status Solidi, Vol. 221, pp. 1-12, 2024. https://doi.org/10.1002/pssa.202400364.

[27] A.N.M. Alahmadi, "Design of an Efficient PTB7:PC70BM-Based Polymer Solar Cell for 8% Efficiency," Polymers (Basel)., Vol. 14, Code: 889, pp. 1-11, 2022. https://doi.org/10.3390/polym14050889.

[28] S. Moulebhar, C. Bendenia, S. Bendenia, H. Merad-Dib, S.A. Khantar, and S. Merabet, "High-efficiency design and optimization of 2 T monolithic polymer/polymer tandem solar cells using SCAPS-1D simulations," Phys. Scr., Vol. 100, pp. 045108(1-12), 2025. https://doi.org/10.1088/1402-4896/adbe03.

[29] D. Raeyani and A. Asgari, "Enhancing the Efficiency of Inverted Organic Solar Cells with Treatment Techniques: Numerical and Experimental Study," Int. J. Energy Res., Vol. 2023, pp. 1-24, 2023. https://doi.org/10.1155/2023/6612574.

Habib Kazemi Chubi, a PhD student in Photonics in State University of Tabriz, is a Lecturer at Osku Azad University, Osku, Iran. His major thrust areas of expertise encompass Photonics and Solar Cells. Formely, he served as a deputy manager at Osku University. He was also the head of Physics Department at Osku Azad University.

Davoud Raeyani received his PhD in photonics from the University of Tabriz, Tabriz, Iran, where he specialized in organic and perovskite optoelectronic devices. His work spans organic, perovskite, and nanomaterials, as well as thin-film optoelectronic devices, with a focus on understanding and engineering charge-transport processes in emerging semiconductor systems. He holds a M.Sc. in Photonic Electronics from the University of Tabriz, where he studied the gas-sensing behavior of graphene quantum dots, and holds a B.Sc. in Solid State Physics from Urmia University, Urmia, Iran. His current research at Instituto de Ciencia de Materiales (ICMUV) Universidad de Valencia, Catedrático José Beltrán, Spain, as a postdoctoral researcher focuses on lead-free perovskite materials for photodetection, memristive, and neuromorphic applications, with the main goal of uncovering the charge-transport mechanisms in these materials for use in next-generation imaging systems.

Asghar Asgari, is a Professor of Physics at the University of Tabriz, Tabriz, Iran. In 2003, he received his Ph.D. degree in Solid State Physics and Electronics from the University of Tabriz (and University of Western Australia). He was a Research Fellow in the field of Microelectronics from 2002 to 2004 at the University of Western Australia. He joined the University of Tabriz, as an academic member in 2004. He is also Adjunct Professor at the University of Western Australia from 2007 until present. He is working on optoelectronic devices.

THIS PAGE IS INTENTIONALLY LEFT BLANK.